Growth and stability of Pb intercalated phases under graphene on SiC

S. Chen,[1] P. A. Thiel,[2,*] E. Conrad,[3] and M. C. Tringides[1,†]

[1]*Department of Physics and Ames Laboratory-U.S. DOE Iowa State University Ames, Iowa 50011, USA*
[2]*Department of Chemistry and Ames Laboratory-U.S. DOE Iowa State University Ames, Iowa 50011, USA*
[3]*Department of Physics, Georgia Technology Institute, 837 State Street Atlanta, Georgia 30332–0430, USA*

(Received 12 December 2019; revised 6 October 2020; accepted 16 November 2020; published 17 December 2020)

Graphene intercalation is a novel way to control graphene's band structure and generate two-dimensional quantum materials with unusual spintronic and electronic properties. Despite its importance, information about the intercalation mechanism is lacking, especially the role of low density domain boundaries between regions of graphene of different thickness. With high resolution surface diffraction we have systematically studied Pb intercalation on epi-graphene grown on SiC, with domain boundaries between buffer and single layer graphene. By examining the evolution of different diffraction spots as a function of tempertature, the location of Pb and stability of the intercalated phases underneath were determined.

DOI: 10.1103/PhysRevMaterials.4.124005

I. INTRODUCTION

As the first two-dimensional (2D) material with the unique band structure of massless electrons and linear energy dispersion, graphene has gained much attention because of its unusual electronic properties [1,2]. One of the most commonly used types of high-quality graphene that has large domain sizes is epi-graphene grown on SiC. It has been extensively studied over the last 15 years. Recently there has been a strong interest to use intercalation to modify graphene's properties by controlling the intercalated metal and the electronic interactions at the graphene-metal interface. Originally intercalation was applied to produce free-standing graphene and to tune the Fermi level position with the intercalated coverage [3–7]. For graphene on reactive metals, intercalation is a robust method to protect them by passivation under ambient conditions [8], harsh gas environments, or high temperature treatment [9].

Intercalated metals have become promising to modify graphene and engineer a large band gap in graphene via spin-orbit (SO) coupling to realize the quantum-spin-Hall-effect state at higher temperatures [10,11]. Intercalating heavy atoms like Pb with large SO coupling was used to modify the energy spectra and density of states of graphene [on Ir(111)] so it becomes equivalent to the energy levels of a 2D electron gas in a constant magnetic field [12]. In Ca-intercalated bilayer graphene, 2D superconductivity was observed [13], thus extending the range of electronic phenomena that can be tuned by intercalation [14,15].

For the case of modifying graphene's properties and generating novel electronic phases, the intercalated metal coverage and location are very important. For example, in Ca-intercalated graphene the intercalated amount should be the coverage of a well-ordered $\sqrt{3} \times \sqrt{3}\mathrm{R}30^\circ$ Ca superstructure, with Ca between the top two layers of bilayer graphene. Pb intercalation was performed in a few cases for graphene on metals (Gr/Ru [9,16,17], Gr/Pt [18], Gr/Ir [12]) and also Gr/SiC (graphene on SiC) [19]. The Gr/SiC system offers more possibilities because different initial graphene thickness can be selected, with a range of intercalated locations (i.e., between buffer layer and SiC, between the top graphene layer and buffer layer, etc.).

The goal of the current paper is to provide more information about the kinetics of intercalation by studying Pb on Gr/SiC for different coverage θ, temperature T, annealing time t_A using spot profile analysis low energy electron diffraction (SPA-LEED). SPA-LEED provides good statistics about the intercalated structures forming in different regions while giving depth profile information [20]. A mixed initial surface is chosen where there is a coexistence between the graphene buffer layer (BL) and single layer graphene (SLG) domains, of large lateral extent, with a very low density of domain boundaries in between. The two regions have different heights because SLG domains consist of a BL plus a top layer of graphene; hence, domain boundaries between BL and SLG domains are steplike. Such domain boundaries can occur at flat or stepped regions on the SiC surface, with changes in the local graphene bonding that can promote intercalation. Because of the high Pb mobility, these boundaries are accessible even at relatively low temperatures. The importance of domain boundaries for graphene intercalation was shown in Ref. [21].

On this mixed Gr/SiC substrate, Pb intercalation happens at a relatively low temperature of $\sim$200 °C. This is indicated by the disappearance of the Pb diffraction spot when the initial Pb islands (formed during deposition) breakup as the Pb moves below the graphene layers. Besides the disappearence of the Pb(10) spot, the other diffraction spots do not recover to their initial intensities of the clean surface. If the Pb atoms had not intercalated but instead simply dispersed to distances

*Deceased.
†Corresponding author: mctringi@iastate.edu

outside the coherence length (the distance probed coherently by SPA-LEED), the LEED diffraction pattern would be identical to the one of the clean surface and the other spots would have recovered to their initial values. As we will demonstrate, details of the SPA-LEED diffraction pattern (intensity, diffraction spot shape, etc.) allow us to measure where the Pb is vertically and its lateral structure. For example, in the previous literature [2] (based on video LEED) superstructure spots commonly referred to as $6\sqrt{3} \times 6\sqrt{3}$ spots, indicate the presence of BL graphene on the SiC surface. The location and amount of the intercalated metal can be deduced from changes in the intensity of such spots with annealing temperature.

The amount of a given graphene phase (i.e., whether BL or SLG) on the surface can be controlled by the annealing temperature and/or time. The average domain size for each phase can be determined from the intensity and shape of the diffraction spots corresponding to the phase. When different phases coexist with domain boundaries separating them, graphene bonding at the domain boundaries differs from the ideal sp^2 bonding, and intercalation will be easier. The deposited atoms can diffuse to the domain boundaries and move below graphene. These insights can be used even to induce the intercalation of slow diffusing atoms, by reducing graphene domain sizes on the initial surface or by increasing the annealing temperature after metal deposition. Manipulating the metal atoms' access to domain boundaries can thus be a general approach to intercalate any metal in controlled and predictive ways.

II. EXPERIMENT

Experiments were carried out in ultra-high vacuum (UHV) at a pressure $\sim 5 \times 10^{-11}$ Torr. The growth of high quality graphene on 4-H SiC(0001) was carried out at high temperatures to desorb Si, while C diffuses and forms large uniform domains [22]. By annealing within 1200 °C–1400 °C, graphene of different thickness can form, starting with the first layer of graphene above the SiC surface (the BL graphene) and finishing with up to a trilayer graphene. In the current experiments short 15-s flashes at 1200 °C were used to control graphene thickness.

Pb was deposited using a flux rate of ~1/25 ML/min at a low sample temperature of −180 °C (liquid nitrogen LN_2). Data were taken for two different coverages; 5 ML and 10 ML. The Pb films were annealed using e-beam heating. Temperature was measured with a Re-W (3%–25%) thermocouple that was calibrated based on the well-known Pb/Si(111) phase transitions [23]. A completely restored clean graphene surface was obtained by heating to 925 °C for 5 min.

The LEED scattering process used in these experiments is described elsewhere [20]. The diffracted intensity is proportional to

$$\mathrm{I}(\boldsymbol{k}_{||}, k_z) = \left| \sum A_n e^{i(\boldsymbol{k}_{||} \cdot \boldsymbol{r}_n + k_z \cdot z(\boldsymbol{r}_n))} \right|^2, \quad (1)$$

where $(r_n, z(\mathbf{r}_n))$ is the position of the n$^{\text{th}}$ atom and A_n its scattering factor. The momentum transfer $\mathbf{k}$ is $\mathbf{k} = \mathbf{k}_f - \mathbf{k}_i$ where $\mathbf{k}_i$ and $\mathbf{k}_f$ are the incident and scattered electron momentum. In this work, we are interested in the momentum transfer parallel to the surface, $k_{||}$.

The electron energy used for the LEED was chosen in the majority of the experiments to be either 100 or 62 eV. The 100-eV energy is optimal to record a 2D pattern with all spots present, while the 62-eV energy maximizes the sensitivity to intercalated Pb between graphene layers.

III. RESULTS

Diffraction pattern of Gr/SiC after Pb deposition. Figure 1(a) shows a schematic of the 2D Brillion zone (BZ) of the graphene-SiC system and the location of diffraction spots from SiC and graphene. The graphene hexagonal BZ is rotated 30° relative to the SiC BZ. Superstructure spots are also visible. The origin of these spots is complicated and has been actively investigated over the years, defining the

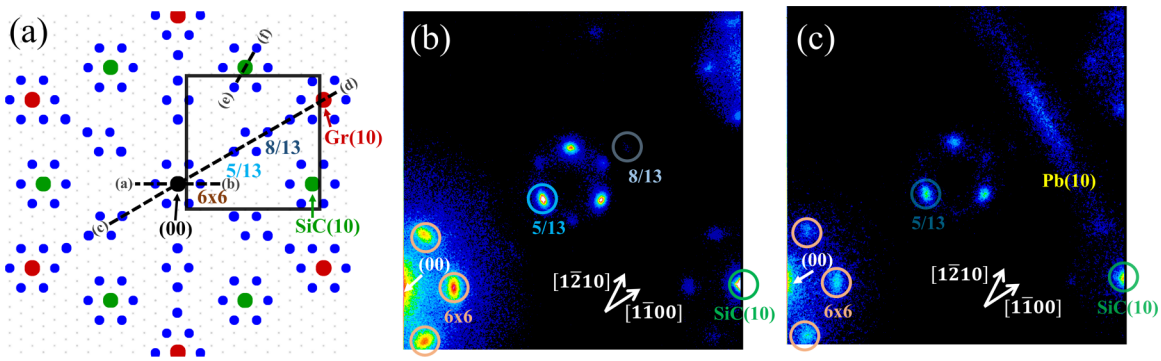

FIG. 1. (a) Schematic of the diffraction pattern of graphene grown on SiC(0001). Red spots are the (1 × 1) graphene spots, green spots are the (1 × 1) SiC spots, and blue spots are the superstructure spots of the graphene-SiC system. The black square shows the experimental area probed in (b) and (c). Black dashed lines show profile directions, "ab" for the one in Fig. 3(b), "cd" for the ones in Figs. 2 and Fig. 3(a) and "ef" for the one in Fig. 5. (b) Experimental diffraction pattern from a surface with a mixture of buffer layer (BL) and single layer graphene (SLG) (E = 100 eV). The 2D area of the BZ is centered around the graphene 5/13 superstructure spot triangle. The SiC crystallographic directions are marked and the 5/13 and 8/13 spots are circled. (c) Diffraction pattern [same region as (b)] after a 10 ML Pb deposition at −180 °C. (E = 100 eV). A Pb(10) arc from an orientational distribution of Pb islands is visible. The center of the arc is on the [1$\bar{1}$00] direction indicating that this is the preferred island orientation.

nomenclature used by the community. They were assigned to a $6\sqrt{3} \times 6\sqrt{3}$ superstructure of commensurate (13 × 13) graphene supercell on SiC, which also consists of three 6 × 6 unit cells oriented along the SiC directions. Recently it was shown that the superstructure spots are due to an incommensurate structure between the BL and the top SiC bilayer with deviations of graphene bonding distances at the graphene-SiC interface [24]. The six spots around the SiC and the graphene fundamental spots are referred to as the 6 × 6 spots. In this paper, we will use the commensurate notation because it is simpler. Regardless of the exact model for the BL-SiC interface, different spots are sensitive to different phases present and more importantly to the Pb location after it intercalates.

The first layer grown on SiC, the BL, is measured by the intensity of the superstructure spots [see Fig. 1(b)]. Similarly the intensity of the Gr(10) spot is proportional to the area of the graphene layer above the BL in the SLG area. Finally, the intensity of the Pb(10) spot is proportional to the Pb island coverage on top. The Pb(10) spot extinction is a sign of Pb intercalation between graphene layers. Monitoring any given spot after the Pb(10) spot becomes extinct, allows us to determine the intercalated area that is proportional to that spot's intensity. For example the SiC(10) spot is sensitive to the BL-SiC interface area. Note that the Pb islands have a distribution of orientations relative to graphene. This is shown in Fig. 1(c) where the Pb(10) spot appears as an arc. The center of the arc is on the $[1\bar{1}00]$ direction indicating that this is the preferred island orientation, i.e., the Pb unit cell is along the graphene unit cell. The analysis of all the diffraction spots allows us to extract key parameters [integrated areas, full width at half maximums (FWHMs), and functional forms used to fit the profile] that are used to determine the real space morphology and the area covered by the different graphene layers.

Controlling the initial graphene G/SiC morphology. Varying one of the three control variables θ, T, t_A can change the total amount of Pb intercalation, its location, and its ordering. Figure 1(b) shows a 2D BZ area centered at the triangle formed by the 5/13 spot and its neighboring 6 × 6 spots. These spots will attenuate faster as the fractional area of the exposed BL is reduced; when the graphene monolayer grows above it to complete the SLG. This transformation occurs when the sample is annealed at ∼1300 °C. The (00) spot and the surrounding 6 × 6 spots are seen at the bottom left in Fig. 1(b). When the graphene thickness is several layers (after annealing to ∼1400 °C), the intensity of these spots decreases more slowly, but eventually disappears for multilayer graphene. Fig. 1(c) shows the surface after Pb deposition at −180 °C. To follow the structure of the Pb intercalation, we will concentrate on diffraction line profiles along certain paths through the BZ. Schematics of these paths are shown in Fig. 1(a), "ab" for the profile in Fig. 3(b), "cd" for the profiles in Fig. 2 and Fig. 3(a) and "ef" for the profile in Fig. 5.

Figure 2 shows scans along the $[1\bar{1}00]$ direction [the "cd" from Fig. 1(a)]. The lower scan in Fig. 2 (black) corresponds to the starting graphene SiC surface (prepared at 1200 °C). The diffraction from the starting surface consists of a strong superstructure 5/13 spot and a weak Gr(10) peak. The narrow Gr(10) component in Fig. 2, indicates the formation of SLG areas above the BL that have well-separated BL-SLG domain

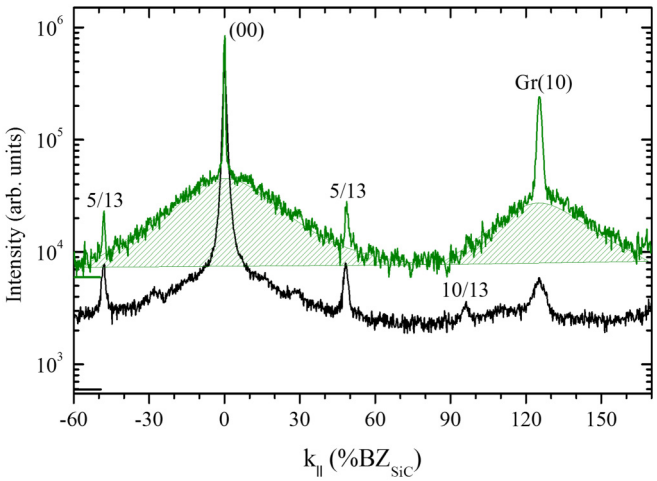

FIG. 2. SPA-LEED profiles along the $[1\bar{1}00]$ direction through the (00) rod and the Gr (10) spot ($E = 194$ eV). The intensity scale is logarithmic and the top (green) curve is shifted upwards relative to the bottom (black) curve. The shift is marked by the long horizontal (green and black) bars that correspond to the same intensity of 600 counts. The lower (black) curve is from the initial surface grown at 1200 °C used in the current studies that consists of a mixture of BL and SLG. The green scan corresponds to heating SiC to 1300 °C with essentially a complete SLG forming covering the BL below. The scan shows a strong Gr(10) peak, strong BSC background (shaded), and a weak 5/13 spot measured from the green bar on the ordinate axis.

boundaries. When the BL surface is heated to 1300 °C, the Gr(10) peak becomes more intense while the 5/13 spot drops in intensity (see the top scan in Fig. 2 in green. The top curve is shifted with respect to the bottom one as shown by the small bars of the same intensity on the ordinate axis). Note that the buffer layer spot 5/13 is still visible even though the BL is completely covered by graphene. This is because at the higher 194-eV electron energy, electron attenuation is low that the LEED still probes the burried BL-SiC interface (the effect is well known from other graphene growth studies [2]).

In addition to the peaks, a very broad background labeled the broad bell-shaped component (BSC) forms around both the (00) and Gr(10) spots (shaded curve in Fig. 2). As noted the top profile was grown under conditions which are consistent with a completed graphene film as determined previously [2]. Furthermore, we find that as the pristine BL surface is annealed, both the Gr(10) and the BSC components grow proportionally. Therefore, the BSC is both an indicator of the growth of SLG patches and a measure of the amount of SLG present on the surface [25].

Figure 2 demonstrates not only how the SLG+BL mixture can be tuned by the annealing temperature, but also how analysis of the diffraction spot profiles gives quantitatively information about the structure and relative mixture of BL and SLG. At the lower 1200 °C temperature, the Gr(10) spot is weak compared to the 1300 °C growth temperature. The Gr(10) spot in the predominantly BL film has a FWHM that is three times larger than the FWHM of the Gr(10) spot from the essentially complete SLG film. Since the inverse of the FWHM is a measure of the average domain size, the larger FWHM of the predominantly BL film suggests that the SLG

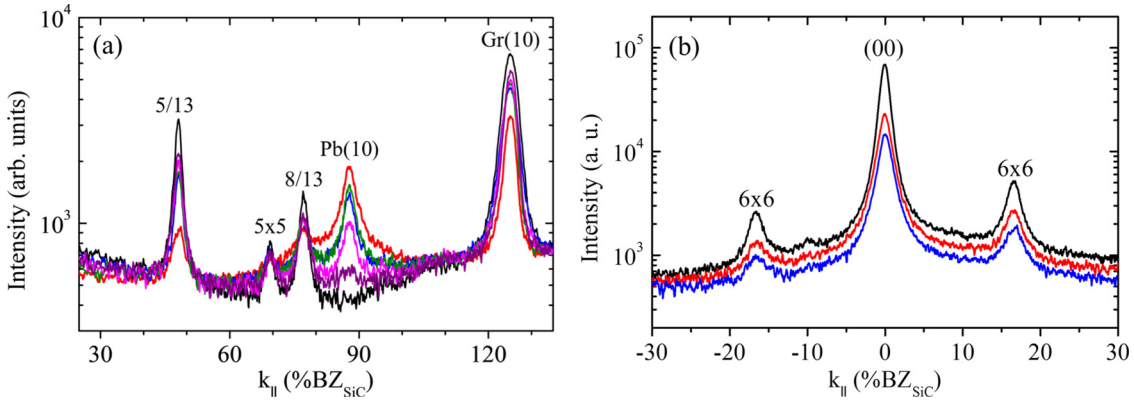

FIG. 3. SPA-LEED profiles through different regions of the BZ. (Electron energy is 62 eV.) (a) Profiles along the [1$\bar{1}$00] direction [scan "cd" in Fig. 1(a)]. The scans are for (black) starting surface, (red) after 5-ML Pb deposition at −180 °C, and the ones in-between after annealing to 50 °C (green), 100 °C (blue), 150 °C (pink), 200 °C (violet) for 30 s; the last one indicates extinction of the Pb(10) spot. The spot to the left of the 8/13 is a 5 × 5 spot commonly present when BL graphene has formed. (b) Profiles along the [1$\bar{2}$10] direction [dashed "ab" line in Fig. 1(a)]. (Black) starting surface, (red) after 5-ML Pb deposition at −180 °C, and (blue) after 10-ML Pb deposition at −180 °C.

graphene domains in the BL film are ∼1/3 the size of the SLG grown at 1300 °C. These smaller SLG patches are surrounded by uncovered BL regions. All of the Pb intercalation experiments in this work were carried out on the mostly BL graphene surface (bottom profile in Fig. 2). The analysis of how the profile fitting is used to determine the detailed morphology of the initial surface depending on growth temperature and time will be published in a future publication. None of the conclusions presented in the current work are affected.

Annealing, intercalation, and recovery of the spot intensity. Figure 3 shows scans along the "ab" and "cd" dashed lines [marked schematically in Fig. 1(a)] for different Pb depositions. After 5 ML of Pb is deposited at −180 °C, a Pb(10) spot forms as seen in Fig. 3(a). The center of the spot is along the [1$\bar{1}$00] direction at 88% of the BZ [consistent with the Pb(111) lattice constant of $a = 0.35$ nm]. The Pb(10) intensity is distributed along a broad arc perpendicular to the [1$\bar{1}$00] direction [see Fig. 1(c)]. The arc's intensity is maximal where it crosses the [1$\bar{1}$00]. Intensity along the arc decreases from its center and still has finite intensity as it crosses the [1$\bar{2}$10] direction close to the SiC(10) spot. The presence of the arc indicates a distribution in the island orientation at this low temperature [26]. Despite the low intensity of the Pb(10) arc near the SiC(10) spot, the arc's proximity to the SiC(10) rod is very fortunate. This effect allows us to simultaneously monitor the relative Pb and SiC diffraction signal as a function of surface annealing.

Two Pb coverages, 5 and 10 ML, were used in these studies. As known from Refs. [27,28] the growth of Pb (and practically all other metals on graphene) is 3D with multiheight islands forming, even at −180 °C deposition temperature. No Pb wetting layer has ever been observed between the islands. Figure 3(b) shows a scan along [1$\bar{2}$10] after low temperature Pb deposition. The (00) and 6 × 6 spots decay in intensity, as the Pb surface layer in the form of Pb(111) islands on top, attenuates the electron beam. An electron energy of 62 eV was used because it makes the diffraction intensity more sensitive to Pb coverage. At the same time Fig. 3(a) shows that the Gr(10) and 5/13 spots also decay in intensity as the Pb islands attenuate the electron beam.

Figure 3(a) shows the evolution of profiles along the [1$\bar{1}$00] direction (through the Pb(10) spot) with annealing: for the initial clean surface (black), after 5 ML deposition at −180 °C (red) and after annealing to 50 °C (green), 100 °C (blue), 150 °C (pink), 200 °C (violet) for 30 s intervals. After the 200 °C annealing step, the strong Pb(10) peak in Fig. 3(a) disappears as seen from the intensity drop by a factor of ∼15 from its initial value. This signifies that Pb has either intercalated under graphene; or that the Pb islands have coarsened to large, well-separated islands. As we now show, only intercalation explains all of the diffraction data.

Diffraction collects information about the surface within the coherence length L of the instrument; for SPA-LEED, $L \sim 300$ nm. Because of the high Pb mobility at 200 °C, if the Pb islands have coarsen they will be separated by macroscopic distances larger than L. Such large multiheight Pb islands would be very few within the illuminated area and would not contribute significantly to the Pb(10) diffracted intensity. In other words, any contribution to the diffracted intensity from these well separated islands that formed on top of the graphene film would be negligible and incompatible with the observed intensity drops of the (00), Gr(10), 5/13, etc., spots and the absence of the Pb(10) spot. The LEED pattern would look identical to the initial clean surface and all the other spots [00, Gr(10), 5/13 etc.] would have returned to their initial clean values, since all the Pb atoms on the surface would be outside L. Pb atoms outside L essentially are not included in the diffracted intensity and thus would not remove intensity from any of the spots. On the contrary as Fig. 3(a) clearly shows, the Gr(10), 5/13, and 8/13 spot intensities are lower at 200 °C from their clean values. This implies that the Pb must have intercalated below either the BL or under the SLG areas. To determine the most stable location of the intercalated Pb, we carried out additional annealing experiments to higher temperatures.

Figure 4 shows the effects of annealing a 5-ML Pb film on the (00) profiles along the [1$\bar{2}$10] direction. Annealing was

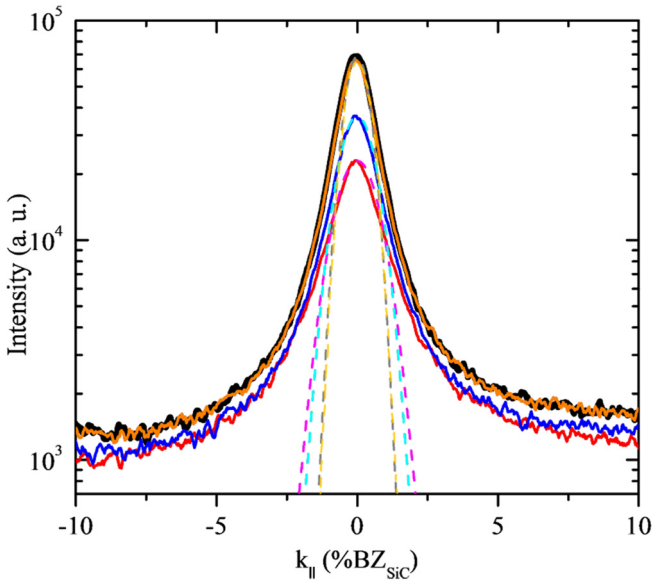

FIG. 4. Profiles of the (00) spot as a function of annealing temperature 100, 450 °C. Scans were taken at an electron energy of 62 eV, along [1$\bar{2}$10]. Black is the profile from the clean surface and gold is the profile after the last 450 °C annealing. Red is the profile after 5-ML Pb deposition at −180 °C. Blue is the profile after the first 100 °C annealing. The gold is identical to the black profile showing partial deintercalation and surface recovery back to its clean surface (00) intensity. The dashed lines are the fits to the central part of the profile fitted with Gaussian function used to monitor the Pb coverage. The profile shapes are similar and the profile FWHMs are constant.

done in 30 s intervals for a series of temperatures between 100 °C and 450 °C. We point out that the effect of annealing on all diffraction spots G(10), 6 × 6, etc., except SiC(10) is the same as on the (00) spot discussed below. Because these spots evolve in a very similar way with annealing, they are not included in the main text but are shown in Supplemental Material Figs. S1, S2, S3. The initial SPA-LEED profile from the clean graphene surface is shown in black in Fig. 4. After 5 ML of Pb was deposited at −180 °C, the profile intensity drops (red curve in Fig. 4). When the film is annealed at 100 °C, the intensity begins to increase (blue curve in Fig. 4). When the annealing temperature is raised to 450 °C, the (00) spot intensity recovers to the clean surface value (gold profile in Fig. 4).

It is common in diffraction to think of the spot profile as consisting of two components; a broad component that is sensitive to short-range order and a narrow central component sensitive to the surface long range order. (For graphene there is also contribution from the BSC). In this experiment the broad component would be a measure of Pb islanding and the narrow component is sensitive to the total Pb coverage [20]. Since all Pb present is below the surface, the narrow central component in Fig. 4 is therefore a good indicator of how much Pb intercalates.

Figure 4 also shows the Gaussian fits to the central peak of the profiles (dashed lines). The range to extract the central Gaussians is chosen to be 20% of the BZ and the background intensity is negligible [29]. We point out that the FWHM of the central peak is constant in these fits. In the Supplemental Material a different fit is used for the central part of the profile; a Lorentzian-3/2 function, shown in Fig. S4. The integrated intensity of the central part of the profiles as a function of annealing temperature is shown in Fig. S5 for the Gaussian and Lorentzian-3/2 functions. The variation with temperature is identical for the two fits confirming that either function is a good representation of the temperature variation of the central component in Fig. 4. This is simply because the central peak intensity is two orders of magnitude larger than the background [29].

The (00) spot intensity drops with the initial Pb deposition, but with increasing annealing temperature the central peak intensity grows. This trend is consistent with the assertion that more of the graphene surface is uncovered as Pb intercalates below. Full intercalation is completed by annealing to 200 °C as already discussed in connection to the extinction of the Pb(10) spot in Fig. 3(a) and that none of other spots have recovered to their initial clean surface values. Further heating to 450 °C fully recovers the (00) spot to its clean surface intensity [and as discussed below of all other spots except SiC(10)]. This indicates that Pb has deintercalated at least from all areas not contributing to the SiC(10) spot. The temperature evolution of the (00) rod is shown in Figs. 4 and S5.

The observation that the FWHMs (used to fit the central part of the profiles in Fig. 4) are independent of annealing is also consistent with the conclusion that the Pb in the surface has first intercalated below graphene, followed by partial deintercalation. The constant FWHM for profiles measured at an out-of-phase condition gives information about how the lateral arrangement of Pb below graphene is changing. If the intercalated atoms below graphene are in a disordered phase, they can lower the (00) central component intensity without affecting the FWHM. The same behavior is known to occur in diffraction profiles from a lattice gas, that only show decrease in the peak intensity without spot FWHM change. Even if the intercalated atoms form clusters the FWHMs must still remain constant. No matter what layer the Pb are intercalated in, the Pb atoms are at nearly the same height $z(r_n)$ above that layer. This means that the phase term $f_n = k_z(z(r_n))$ in Eq. (1) for the nth intercalated atom at location r_n varies only by a small amount as a function of location. From textbook diffraction, the diffraction profile broadens in $k_{||}$ and the FWHM changes only if there is a wide distribution in Pb atom heights $z(r_n)$ [20]. For example, since metal islands at the top of the surface have different height $z(r_n)$ from the substrate atoms, they can cause destructive interference and can change the measured FWHM. The FWHM will then depend on island size. For intercalated atoms in the smooth graphene film, the height variations must be small. Therefore, even for clustered intercalated atoms the FWHM of the profiles in Fig. 4 will be unchanged during annealing.

No Pb disordered phase after annealing. From previous studies of metal growth on graphene the growth mode for all deposited metals was found to be 3D, because the metal-graphene interaction is much weaker than the metal-metal interaction [28]. This favors the deposited metal atoms to join the nucleated islands instead of wetting graphene. After Pb deposition at −180 °C, Pb forms 3D islands and all the deposited atoms join the nucleated islands because the Pb

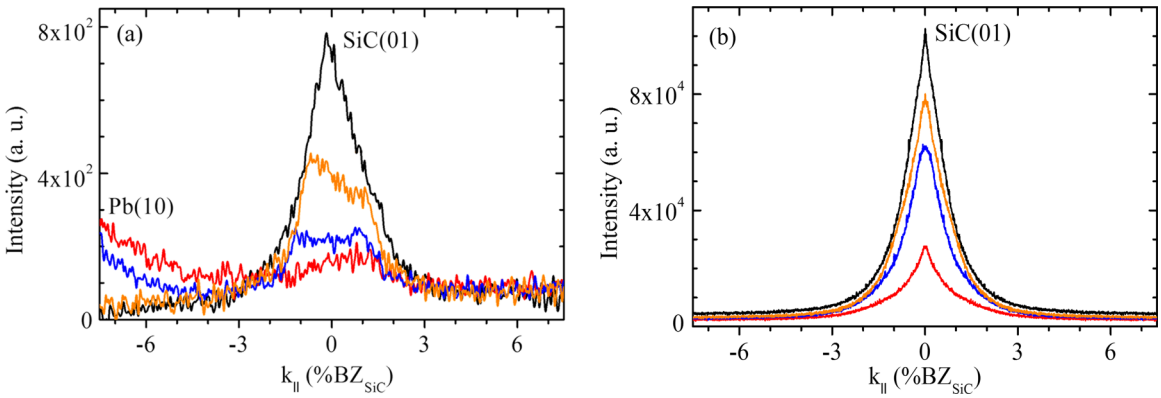

FIG. 5. (a) Profiles of the SiC(10) along [1$\bar{2}$10] electron energy 62 eV as a function of annealing temperature for 5 ML of Pb in the range 100 °C–450 °C with initial surface (black), −180 °C (red) and after annealing to 150 °C (blue) 200 °C (gold).The SiC(10) spot is weak at 62 eV, so a linear intensity scale is shown. The higher intensity to the left (red, blue) is from the lower edge of the Pb(10) arc crossing the [1$\bar{2}$10] direction confirming Pb(10) extinction at 200 °C. After heating to the highest temperature 450 °C, the SiC(10) does not recover and is at ∼80% its initial intensity. Figure 5(b) SiC(10) spot after 5-ML deposition measured at higher electron energy 186 eV initial surface (black), −180 °C (red) and after annealing to 250 °C (blue), 450 °C (gold), showing that after annealing to 450 °C the intensity is also at ∼80% its initial intensity.

mobility is extremely high. No adatoms are seen between the islands [27]. The diffusion barrier of Pb on graphene was measured to be less than 0.035 eV. Based on this barrier and a normal diffusion prefactor $\nu_0 = 10^{13}\,\mathrm{s}^{-1}$ the island separation at 200 °C is found to be 360 nm, which is comparable to the SPA-LEED coherence length. This essentially implies that at 200 °C all the Pb atoms are in Pb crystalline islands with no adatoms in the region between the islands.

The very high Pb diffusion length means that after annealing there are only three possible outcomes: either the Pb islands coarsen to larger sizes, Pb partially desorbs, or Pb partially intercalates. The extinction of the Pb(10) spot [discussed in Fig. 3(a)] cannot be attributed to Pb still being on top of graphene in a disordered state (such as a lattice gas). Any diffusing lattice gas Pb adatom will easily find the islands already present on the surface, and thus will not be the reason for the decrease of the Pb(10) intensity. The diffusion distance a Pb adatom travels (within the coherence length L^2 area), is found from the standard relationship $R = 4Dt^{1/2}$. Using $t = L^2/F = 1.5 \times 10^{-4}$ s (the time between arrivals of two consecutive Pb atoms in L^2 with $F = 1/25$ ML/min as the flux rate) gives $R = 300$ nm at LN_2 and $R = 0.5$ mm at 200 °C. Since $R \gg L$ at 200 °C this again implies a deposited adatom will join the Pb islands already on the surface. This simple estimate shows that no Pb will be on top in a disordered phase to cause the extinction of Pb(10). It follows that Pb atoms still present (as deduced from the spot intensities being below their clean surface intensities) must be below graphene. Although these estimates were made during island growth, it is also seen that annealing experiments will not generate Pb adatoms on graphene coexisting with smaller Pb islands, since any released Pb adatoms are very mobile, will join islands, and give rise to island coarsening [28].

Previous Pb desorption studies on graphene on Ru(0001) in Ref. [9] found that Pb desorption from multilayer Pb islands occur at ∼340 °C while Pb desorption from single layer Pb islands on graphene occurs at ∼580 °C. In the current experiment, the diffraction evidence indicates that the intercalated Pb begins to deintercalate and desorb after annealing at 450 °C. This puts the Pb desorption temperature in this experiment within the range of island desorption temperatures in Ref. [9].

Preferred Pb intercalation under BL in the SLG area. As already discussed, the SiC(10) spot behaves differently from the other diffraction spots. Figure 5(a) shows the profile of the SiC(10) spot after 5-ML Pb deposition. The SiC(10) spot is weaker at an electron energy of 62 eV compared to an energy of 186 eV [Fig. 5(b)]. At 62 eV, the SiC(10) peak intensity is 100 times lower than when using 186 eV. This is due to the shorter elastic mean free path at 62 eV. Since the SiC(10) spot originates from the buried SiC-BL interface, a drop of its intensity from the clean surface value indicates the presence of intercalated Pb. The advantage of using 62 eV in this study is that it enhances the relative intensity of the Pb (10) spot. The intensity from the Pb(10) arc (that crosses the [1$\bar{2}$10] direction) in Fig. 5(a) is clearly visible close to the SiC(10) spot. The Pb(10) arc measures Pb on top and the SiC(10) spot measures the BL-SiC interface. The Pb(10) arc intensity in Fig. 5(a) is no longer visible by annealing at 200 °C. The scans support that 200 °C is the temperature when the Pb(10) arc becomes extinct, as already deduced from the scan along [1$\bar{1}$00] in Fig. 3(a). The extinction of Pb(10) and the SiC(10) intensity being below its clean surface value show that intercalated Pb is present at the BL-SiC interface, the area measured by the SiC(10) spot.

Figure 5(a) shows that after annealing at 450 °C, the SiC(10) spot intensity does not return to the clean surface value. Instead it remains at ∼80% of its initial clean surface intensity. An even lower drop in the SiC(10) intensity (60%) is seen after annealing a 10-ML Pb film at 450 °C. The SiC(10) spot only recovers to its clean surface value after the sample is annealed to at least 700 °C. Figure 5 clearly demonstrates that Pb has intercalated below graphene, attenuating the elastically diffracted electrons from the SiC. We can go

on to show that, not only has the Pb intercalated, we can identify the most stable intercalation location, i.e., the one that is occupied after the annealing to 450 °C. To show this, we look at how intercalation at the other possible locations can be ruled out based on the intensities of the other spots measured.

First we assume that Pb intercalates between the bare BL and SiC. By bare BL, we mean areas of the BL not covered by graphene. Previous intercalation studies have shown that intercalants between BL and SiC cause the BL to convert to graphene, which would increase the Gr(10) intensity [7]. Since the Gr(10) has the same intensity at 450 °C as for the clean surface, we can eliminate Pb intercalation below bare BL. In addition since the 6 × 6 superstructure is associated mainly with the BL, intercalation below bare BL at 450 °C would cause the 6 × 6 spots to decrease, which also is not observed.

Suppose on the other hand, that the Pb intercalates between the BL and graphene in the SLG area. In this case, the intensity from the SLG is no longer that of pristine SLG. We can think of the Pb atoms as "defects" below monolayer graphene, which interrupt the long-range order in SLG. The intensity in Eq. (1) over the SLG contains terms $A_n e^{ikr}$, but now it includes different scattering factors A_C for C and A_{Pb} for Pb atoms. These Pb "defects" would decrease the diffracted intensity of the Gr(10) spot, so it would not be the same as the clean surface. Since the Gr(10) intensity after annealing to 450 °C recovers to the clean surface level, we can rule out intercalation between the graphene top layer and the BL. The only intercalation location consistent with the diffraction data is for the Pb to be intercalated under the BL covered by graphene, as discussed in connection to the SiC(10) drop for Fig. 5. This spot at 450 °C has intensity below its clean value and only recovers at 700 °C. The difference from its initial value is a measure of the intercalated amount under BL in the SLG area.

It is surprising that the 6×6 intensity at 450 °C fully recovers since the 6×6 phase is removed in the SLG area (although as noted this area is a smaller fraction than the BL area and also its intensity is attenuated from the graphene layer on top). Possibly this means that some of the Pb intercalated regions might have 6×6 regions, since this periodicity is close to the periodicity of a 5×5 Pb(111) supercell; or there are still very few bare 6×6 regions of large lateral extent that add to the 6×6 intensity significantly and account for the full recovery.

A concise way to follow the evolution of each spot is to plot the integrated area $I(s)/I(0)$ ratio and the FWHM as a function of annealing temperature T, with $I(s)$ the intensity for intercalated Pb coverage s, and $I(0)$ the intensity of the spot for the clean surface. An example is shown for the (00) spot in Fig. S5 in the Supplemental Material. In such a plot the difference of the spot intensity from the clean surface value is a measure of the intercalated amount with annealing, for temperatures above 200 °C.

The current experiment uses an intensity of different diffraction spots to follow the location of the deposited Pb with annealing temperature from the very first deposition well below room temperature. Further annealing to 450 °C shows Pb has deintercalated from all locations except under BL in the SLG area, which eventually deintercalates at 700 °C . Besides determining the most stable binding location of the intercalated metal, the experiment also maps out the temperature pathway for the metal to move to this most stable location.

IV. DISCUSSION

Candidate intercalation mechanisms. As already discussed, the mechanism of graphene intercalation still poses open questions. It is hard to imagine how the deposited atoms on top can break graphene's in-plane sp^2 bonds and go through the graphene lattice. There is no complete and definite study to identify a universal process that aids intercalation, partially because intercalation is mainly a kinetic process determined by key controlling barriers. It is common in density functional theory studies to assume the presence of defects that facilitate the transfer of atoms from above to below graphene [30]. However, the defect densities required in those studies are much higher than real defect densities in graphene; otherwise such high defect densities would break long-range order and domain homogeneity. This would degrade the promising electronic properties of graphene. A large number of defects can modify its electronic band structure, even causing deviations from the linear energy dispersion and lower electron mobilities. No such high defect densities are seen experimentally. For example mesoscale defects of much lower densities have been identified in some systems using low energy electron microscopy (LEEM). In Gr/Ir(111), thermal stresses related to lattice mismatch and strong graphene substrate interaction, generate "wrinkles" for Cs atoms to move below graphene [31].

Intercalation through domain boundaries. Domain boundaries play a general role in intercalation for many systems, especially ones with high diffusion rates like Pb. They have been shown to be important for Pb intercalation in Gr/Ru(0001) [9]. For graphene grown on metals the initial surface is not fully covered by graphene. Using LEEM, it was shown that a 2D Pb wetting layer forms at the bare Ru(0001) areas and Pb moves from the wetting layer, through the edges of finite graphene domains, to intercalate graphene. This mechanism is only possible for an inhomogeneous system, with incomplete graphene domains coexisting with a partially exposed metal substrate.

Graphene on SiC completely covers the SiC surface, including growing over steps, so that there are no exposed bare regions for a similar mechanism to operate. However, for a mixed system, at the boundaries separating the two phases (BL and SLG), the bonding at the boundary atoms involves both normal and lateral atom displacements from the ideal hexagonal unit cell positions, which on flat areas have perfect sp^2 configuration. These weaken the lateral C bonds at domain boundaries and can lower the barrier for the metal atoms on top to go through and bond to sites below graphene.

An STM study of such a mixed surface at LN_2 temperatures has shown preferred island adsorption on the BL [32]. The preferred adsorption is due to the stronger Pb bonding on BL and higher mobility on the SLG areas that facilitates transfer of material from the top of SLG to the top of the BL area. [Although Ref. [32] focuses on Pb adsorption on top and not

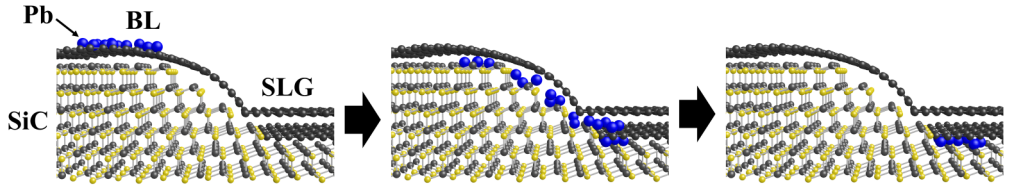

FIG. 6. Schematic of the intercalation process on mixed surface with coexisting single layer graphene (SLG) and buffer layer (BL). The step structure is based on the one deduced in Ref. [33]. It includes a flat area at the edges of the stepped region, with BL at the top and SLG at the bottom region. Graphene at the stepped area is decoupled which allows the metal atoms to move below graphene. Black balls are C, yellow balls are Si, and blue balls are Pb atoms. Pb deposition at LN_2 temperature (left). Transfer of the Pb at 200 °C below seen by the extinction of the Pb (10) spot (middle). Deintercalation after the surface is heated above 200 °C with most of the Pb recovered at 450 °C, except the amount below the BL in the SLG area; since recovery of the SiC(10) spot to its initial value requires higher ∼700 °C annealing (right).

on intercalation below graphene, it is consistent with the larger intensity drop of the 5/13 spot at −180 °C seen in Fig. 3(a), and the smaller drop of the G(10). The 5/13 spot measures the area covered by the BL and since the BL collects more Pb on top, the intensity drops more than the drop of the G(10) spot which measures the graphene area].

For a mixed BL and SLG system there are complex boundaries separating the two phases, especially the ones that involve SiC steps. Detailed information about such boundaries exists in the literature that can be used to understand the intercalation process. A real step structure spontaneously generated on Gr/SiC (or seen in facetted areas grown lithographically) shows flat regions at the top and bottom edges of the steps, while in the middle decoupled graphene grows [33]. Such a structure is sketched in Fig. 6 with BL at the top, decoupled graphene at the middle and SLG at the bottom. Different height steps can be in the facetted region corresponding to different high index SiC planes. Because graphene domains in the stepped areas are decoupled, with weaker bonds to the substrate, they are ideal locations for metal atoms to move below graphene and initiate intercalation. Also as shown recently graphene (both the BL and SLG) is incommensurate with SiC, so there must be either dangling bonds or rehybridized bonds where graphene terminates into the SiC steps, which further weaken the bonding at the domain boundaries [34]. These defects either reduce the strength of the lateral C bonds or insert vacancies at the graphene-SiC step domain boundaries. The graphene-step boundary will, therefore, lower the diffusion barrier for metal atoms above graphene to diffuse to bonding sites below the graphene film. Pb has very high mobility and it can reach these stepped areas (even when they are only a fraction of all domain boundaries and are well separated). These areas can be the entry portals for metal atoms to move below.

A different study has shown that 3D protrusions develop at various stages of the SiC graphitization [35] as gradually the $6\sqrt{3} \times 6\sqrt{3}$ areas convert to SLG. The top of the protrusions is draped by SLG and the lower side by BL domains. The edges of the protrusions expand laterally and the draped SLG layer grows as the $6\sqrt{3} \times 6\sqrt{3}$ to SLG transformation proceeds to eventually complete the full SLG. A small fraction of such protrusions can still remain on the surface as metastable, kinetically limited structures, after the transformation is completed. Because edges of such protrusions are different types of domain boundaries between BL and SLG and have interrupted sp^2 bonding, this is another avenue for the metal atoms to diffuse through them and move below graphene.

Figure 6 shows schematically the outcome of intercalation at domain boundaries between BL and SLG on stepped structures identified in Ref. [33]. Initially Pb is deposited on top and nucleates islands mostly in the BL area (left). Intercalation can proceed through the stepped areas because graphene is weakly coupled in these regions and metal atoms can move underneath graphene (middle). After annealing to 450 °C the intercalated Pb atoms are bonded mostly under the BL in the SLG area as discussed earlier (right). This is evidenced by the larger drop of the SiC(10) intensity which persists above 450 °C; while the intensity of the other spots being monitored [(00), Gr(10), 6×6] recovers to its initial level of pristine surface. Since these other spots measure Pb bonding to other layers above the buried SiC interface in the SLG area, i.e., between BL and graphene in the SLG area and above BL in the bare buffer layer area, one deduces the only possible Pb location above 450 °C is below BL in the SLG area. If Pb was intercalated in the bare BL area, it would have converted the BL to SLG in this area, which would have increased the Gr(10) spot intensity; this is not observed since the Gr(10) does not grow larger than its initial value. The last region to be recovered is the region at the BL-SiC interface in the SLG area, as seen by the SiC(10) intensity recovering to its initial level at higher temperature ∼700 °C.

By selecting the initial substrate morphology to be a mixture of BL and SLG with domain boundaries between the two areas, Pb intercalation is possible at relatively low temperature ∼200 °C. The importance of domain boundaries for intercalation, has been shown for hydrogen intercalation/deintercalation of Gr/SiC with LEEM [21]. At least two different types of domain boundaries are possible, either between graphene layers of different thickness or antiphase boundaries within the same layer thickness, but of different stacking (AB or AC in adjacent areas) In Ref. [21]. these antiphase boundaries were imaged and real time movies during deintercalation show the receeding hydrogen front below graphene, as hydrogen resurfaces to the top and desorbs. Antiphase boundaries are naturally present in graphene and generate domain walls. The atoms within these walls are at the same height and distort the sp^2 bonding less than the domain boundaries between layers of different thickness, discussed in the current work. Because of the larger sp^2 distortion, domain boundaries between graphene of different thickness will be easier entry portals for intercalation.

In addition the importance of domain boundaries are seen when the current experiments are compared to the Pb intercalation experiments of Ref. [19]. Intercalation in Ref. [19] was carried out on a homogeneous SLG phase, corresponding to the top profile in Fig. 2, which has much stronger Gr(10) spot. Higher annealing temperatures were used in Ref. [19] than in our work since the SLG phase has a much smaller number of domain boundaries. Intercalation was attributed to Pb diffusion through graphene covering SiC steps and transfer of Pb below graphene. In addition in Ref. [19] local patches of an ordered $\sqrt{3} \times \sqrt{3}$ Pb structure were found with STM for the intercalated Pb. There is no evidence of this $\sqrt{3} \times \sqrt{3}$ ordered phase in our experiments, either because the domains are small to be seen by diffraction or because the starting surface is different.

In the current studies on the mixed SLG and BL surface, shown by the bottom profile in Fig. 2 the full recovery of the diffraction spot intensity implies both deintercalation and desorption at 700 °C, so the surface returns back to its initial state. The temperatures where we observe this recovery are consistent with thermal programmed desorption of the Pb-intercalated Gr/Ru(0001) surface. After Pb moves from below to the top of graphene, its desorption temperature is determined by its bonding to the graphene layer irrespectively of whether the graphene is grown on SiC or Ru(0001), so a similar desorption temperature is seen in the current studies as in Ref. [9].

V. CONCLUSIONS

In this work, we have studied the intercalation of Pb at the epitaxial graphene-SiC interface. The intercalation was studied as a function of annealing temperature using SPA-LEED. The experiments presented here are on a mixed BL plus SLG film. From changes in both the intensity and shape of a number of diffraction spots from graphene, SiC, and the interface buffer layer-SiC, we deduce the location and stability of the intercalated Pb. We show that Pb deposited on the surface of this mixed film fully intercalates at 200 °C. Further annealing of the intercalated Pb to 450 °C causes the Pb to deintercalate from all locations except from under regions of the BL that are covered with a SLG film. This implies that the most stable intercalation location for Pb is between the BL and SiC in the SLG areas. At 700 °C, all of the Pb deintercalates and desorbs from the surface.

By comparing with the intercalation literature of the pure SLG, we deduce that most likely intercalation in the mixed system is through the domain boundaries, especially the ones at SiC steps. These BL+SLG domain boundaries are easily accessible because of the high Pb mobility. Because the BL graphene is incommensurate with the SiC, the graphene sp^2 bonding is highly distorted lowering the intercalation barrier when compared to the barrier for the flat, undistorted surface. The sp^2 bond distortion at these boundaries is much more likely to allow Pb intercalation at higher rate, than at antiphase boundaries known to be entry portals for hydrogen intercalation. Absence of domain boundaries in studies of Pb intercalation on a uniform SLG layer requires higher intercalation temperatures. The results presented in this work provide a general method of intercalation for any metal on the graphene-SiC system. The domain boundary density can be adjusted by the annealing temperature and time used to grow graphene, so the distance between domain boundaries is comparable to the diffusion length of any deposited metal. This will allow the metal to easily reach the domain boundaries and use them as facile entries for intercalation below graphene.

ACKNOWLEDGMENTS

This work was supported by the US Department of Energy (DOE), Office of Science, Basic Energy Sciences, Materials Sciences and Engineering Division. The research was performed at the Ames Laboratory, which is operated by (Iowa State University under Contract No. DE-AC02-07CH11358.

[1] A. H. Castro Neto, F. Guinea, N. M. R. Peres, K. S. Novoselov, and A. K. Geim, Rev. Mod. Phys. **81**, 109 (2009).

[2] C. Berger, Z. Song, T. Li, X. Li, A. Y. Ogbazghi, R. Feng, Z.Dai, A. N. Marchenkov, E. H. Conrad, P. N. First, and W. A. de Heer, J. Phys. Chem. B **108**, 19912 (2004).

[3] B. Premlal, M. Cranney, F. Vonau, D. Aubel, D. Casterman, M. M. De Souza, and L. Simon, Appl. Phys. Let. **94**, 263115 (2009).

[4] I. Gierz, T. Suzuki, R. T Weitz, D. S. Lee, B. Krauss, C. Riedl, U. Starke, H. Höchst, J. H. Smet, C. R. Ast, and K. Kern, Phys. Rev. B **81**, 235408 (2010).

[5] Y. Dedkov and E. Voloshina, J. Phys.: Condens. Matter **27**, 303002 (2015).

[6] J. Baringhaus, A. Stöhr, S. Forti, S. A. Krasnikov, A. A. Zakharov, U. Starke, and C. Tegenkamp, Appl. Phys. Lett. **104**, 261602 (2014).

[7] P. Rosenzweig, H. Karakachian, S. N. Link, K. Küster, and U. Starke, Phys. Rev. B **100**, 035445 (2019).

[8] A. Lii-Rosales, Y. Han, K. M. Yu, D. Jing, N. Anderson, D. Vaknin, M. C. Tringides, J. W. Evans, M. S. Altman, and P. A. Thiel, Nanotechnology **29**, 505601 (2018).

[9] L. Jin, Q. Fu, R. Mu, D. Tan, and X. Bao, Phys. Chem. Chem. Phys. **13**, 16655 (2011).

[10] M. Zhou, W. Ming, Z. Liu, Z. Wang, P. Li, and F. Liu, PNAS **111**, 14378 (2014).

[11] A. V. Matetskiy, S. Ichinokura, L. V.Bondarenko, A. Y. Tupchaya, D. V. Gruznev, A. V. Zotov, A. A. Saranin, R. Hobara, A. Takayama, and S. Hasegawa, Phys. Rev. Lett. **115**, 147003 (2015).

[12] F. Calleja, H. Ochoa, M. Garnica, S. Barja, J. J. Navarro, A. Black, M. M. Otrokov, E. V Chulkov, A. Arnau, A. L. Vázquez de Parga, F. Guinea, and R. Miranda, Nat. Phys. **11**, 43 (2015).

[13] S. Ichinokura, K. Sugawara, A. Takayama, T. Takahashi, and S. Hasegawa, ACS Nano **10**, 2761 (2016).

[14] K. Kanetani, K. Sugawara, T. Sato, R. Shimizu, K. Iwaya, T. Hitosugi, and T. Takahashi, Proc. Natl. Acad. Sci. USA **109**, 19610 (2012).

[15] K. Li, X. Feng, W. Zhang, Y. Ou, L. Chen, K. He, L. L. Wang, L. Guo, Q. X. Xue, and X. Ma, Appl. Phys. Lett. **103**, 062601 (2013).
[16] L. Jin, Q. Fu, Y. Yang, and X. Bao, Surf. Sci. **617**, 81 (2013).
[17] X. Fei, L. Zhang, W. Xiao, H. Chen, Y. Que, L. Liu, K. Yang, S. Du, and H.-J. Gao, J. Phys. Chem. C **119**, 9839 (2015).
[18] I. I. Klimovskikh, M. M. Otrokov, V. Y. Voroshnin, D. Sostina, L. Petaccia, G. Di Santo, S. Thakur, E. V. Chulkov, and A. M. Shikin, ACS Nano **11**, 368 (2017).
[19] A. Yurtsever, J. Onoda, T. Iimori, K. Niki, T. Miyamachi, M. Abe, S. Mizuno, S. Tanaka, F. Komori, and Y. Sugimoto, Small 3956 (2016).
[20] M. Henzler, Surf. Sci. **132**, 82 (1983).
[21] T. A. de Jong, E. E. Krasovskii, C. Ott, R. M. Tromp, S. J. van der Molen, and J. Jobst, Phys. Rev. Mater. **2**, 104005 (2018).
[22] M. Hupalo, E. H. Conrad, and M. C. Tringides, Phys. Rev. B **80**, 041401(R) (2009).
[23] S. Stepanovsky, M. Yakes, V. Yeh, M. Hupalo, and M. C. Tringides, Surf. Sc. **600**, 1417 (2006).
[24] F. Wang, M. Nevius, K. Jinkins, A. Celis, M. N. Nair, A. Taleb-Ibrahimi, A. Tejeda, Y. Garreau, A. Vlad, A. Coati, P. F. Miceli, and E. H. Conrad, Nano Lett. **17**, 341 (2017).
[25] S. Chen, M. Horn von Hoegen, P. A. Thiel, and M. C.Tringides, Phys. Rev. B **100**, 155307 (2019).
[26] M. Yakes and M. C. Tringides, J. Phys. Chem. A **115**, 7096 (2011).
[27] M. Hupalo, X. Liu, C. Wang, W. Lu, Y. Yao, K. Ho, and M. C. Tringides, Adv. Mater. **23**, 2082 (2011).
[28] X. Liu, C. Z. Wang, M. Hupalo, K. M. Ho, and M. C. Tringides, Crystals **3**, 79 (2013).
[29] See Supplemental Material at http://link.aps.org/supplemental/10.1103/PhysRevMaterials.4.124005 for different fitting functions (Gaussian or Lorentzian-3/2) for the narrow component of the profiles giving similar results for the normalized integrated areas and FWHMs.
[30] L. Huang, Y. Pan, L. Pan, M. Gao, W. Xu, Y. Que, H. Zhou, Y. Wang, S. Du, and H.-J. Gao, Appl. Phys. Lett. **99**, 163107 (2011).
[31] M. Petrović, I. Šrut Rakić, S. Runte, C. Busse, J. T. Sadowski, P. Lazić, I. Pletikosić, Z.-H. Pan, M. Milun, P. Pervan, N. Atodiresei, R. Brako, D. Šokčević, T. Valla, T. Michely, and M. Kralj, Nat. Commun. **4**, 2772 (2013).
[32] X. T. Liu, T. W. Hu, Y. P. Miao, D. Y. Ma, P K. Chu, F. Ma, and K. W. Xu, J. Appl. Phys. **117**, 065304 (2015).
[33] I. Palacio, A. Celis, M. N. Nair, A. Gloter, A. Zobelli, M. Sicot, D. Malterre, M. S. Nevius, W. A. de Heer, C. Berger, E. H. Conrad, A. Taleb-Ibrahimi, and A. Tejeda, Nano Lett. **15**, 182 (2015).
[34] A. L. Miettinen, M. S. Nevius, W. Ko, M. Kolmer, A.-P. Li, M. N. Nair, B. Kierren, L. Moreau, E. H. Conrad, and A. Tejeda, Phys. Rev. B **100**, 045425 (2019).
[35] S. W. Poon, W. Chen, A. T. S. Wee, and E. S. Tok, Phys. Chem. Chem. Phys. **12**, 13522 (2010).